Steidl, Matthias; Wu, Mingjian; Peh, Katharina; Kleinschmidt, Peter; Spiecker, Erdmann; Hannappel, Thomas:

Impact of N incorporation on VLS growth of GaP(N) nanowires utilizing UDMH

Original published in:

Nanoscale research letters : NRL. - New York, NY [u.a.] : Springer. - 13 (2018), art. 417, 9 pp.

Original pulished: December 29, 2018

ISSN: 1556-276X

DOI: 10.1186/s11671-018-2833-6

[*Visited:* January 09, 2019]

Nanoscale Research Letters

NANO EXPRESS Open Access

Impact of N Incorporation on VLS Growth of GaP(N) Nanowires Utilizing UDMH

Matthias Steidl[1*], Mingjian Wu[2], Katharina Peh[1], Peter Kleinschmidt[1], Erdmann Spiecker[2] and Thomas Hannappel[1*]

Abstract

III–V nanowires (NWs) possess great potential for use in future semiconductor technology. Alloying with dilute amounts of nitrogen provides further flexibility in tuning their material properties. In this study, we report on successful in situ nitrogen incorporation into GaP(N) NWs during growth via the Au-catalyzed vapor-liquid-solid (VLS) mechanism. The impact of the nitrogen precursur unsymmetrical dimethyl hydrazine (UDMH) on morphology was found to be overall beneficial as it strongly reduces tapering. Analysis of the crystal structure of NWs with and without N reveals zinc blende structure with an intermediate amount of stacking faults (SF). Interestingly, N incorporation leads to segments completely free of SFs, which are related to dislocations transverse to the growth direction.

Keywords: III–V nanowires, Dilute nitride, Vapor-liquid-solid growth, Mixed dislocations, Stacking faults

Introduction

III–V nanowires (NWs) have attracted considerable interest as building blocks in almost all fields of semiconductor technology [1–4]. In particular, their small footprint allows for efficient elastic strain relaxation [5] and hence for high crystallinity during heteroepitaxy even if the lattice mismatch is tremendous [6]. This opens a very wide field of material combinations, which are hard to realize with high crystallinity in planar heteroepitaxy. Accordingly, restrictions ruled by the requirement of lattice-matching are reduced, and emphasis can be focused on the engineering of optoelectronical, chemical, and structural properties of the NWs.

Alloying conventional III–V materials with nitrogen constitutes so-called dilute nitride compounds and has been proven to be a strong method to further tailor the material properties [7, 8]. For instance, it leads to a strong reduction of the band gap and a transformation of the indirect band gap of GaP to a quasi-direct one when incorporating more than ca. 0.5% of N [9, 10]. Moreover, dilute amounts of N in GaAs, GaP, and InGaP are reported to significantly improve the chemical stability in aqueous solutions [11, 12], which is of great interest for solar water splitting, where photocorrosion is a serious issue.

N-containing GaP NWs were prepared in the past by sublimation and recondensation of ball-milled GaP powder utilizing NH_3 as N source [13]. More recently, molecular beam epitaxy (MBE) growth of various different N-containing III–V-core-shell structures has been demonstrated [14–19]. In these studies, commonly a N-free NW core was grown via the vapor-liquid-solid (VLS) growth mode with a Ga droplet as catalyst (known as self-catalyzed growth mode), and subsequently, a dilute nitride shell was grown by conventional layer epitaxy (vapor-solid mechanism). These studies revealed the great potential of dilute nitride NWs and discovered beneficial properties related to their architecture, such as decreased surface recombination [20], increased light harvesting via energy up-conversion [21], and emission of linearly polarized light [22, 23].

Nevertheless, dilute nitride materials continuously suffer from strong non-radiative recombination, an issue which is known to be closely related with the formation of defects, such as interstitials, antisites, vacancies, and impurity atoms [24–27]. Their formation in turn strongly depends on conditions and parameters applied during growth. For example, hydrogen appears

* Correspondence: matthias.steidl@tu-ilmenau.de; thomas.hannappel@tu-ilmenau.de
[1]Department of Photovoltaics, Institute of Physics and Institute of Micro- and Nanotechnologies, Technische Universität Ilmenau, 98693 Ilmenau, Germany
Full list of author information is available at the end of the article

to promote the formation of point defects [28], and the choice of precursors and epitaxy method has a significant impact on defect formation [26, 29]. Since the VLS-growth of NW (cores) significantly differs from vapor solid growth of layers (or shells), the density of detrimental point defects might be reduced applying the VLS growth mechanism. So far, VLS growth of dilute nitrides was only achieved by self-catalyzed growth [18, 19], which is however restricted by small growth windows. Therefore, parameters have to be carefully tuned and well-defined doping is very challenging [30, 31]. Moreover, this growth mode frequently struggles with parasitic island growth and inhomogeneous NW dimensions [18, 19]. In contrast, Au-catalyzed VLS NW growth is very versatile and rather easy to control and allows for precisely tunable and high doping levels [1, 31–33]. First attempts reported in the literature to prepare dilute nitride NWs via Au-catalyzed VLS growth have, however, not been successful as the N-precursor suppressed one-dimensional growth [34].

In this study, we demonstrate successful dilute nitrogen incorporation via the Au-catalyzed VLS-growth mechanism. We find incorporation of N on group V sites and an overall advantageous impact on morphology and crystal structure by the utilization of the nitrogen precursor unsymmetrical dimethyl hydrazine (UDMH).

Methods

GaP(N) NWs were grown by the Au-catalyzed vapor-liquid-solid (VLS) growth mode on GaP(111)B substrates via metalorganic vapor phase epitaxy (MOVPE, Aixtron AIX 200). Only liquid precursors were used with trimethylgallium (TMGa), tertiarybutylphosphine (TBP), and unsymmetrical dimethylhydrazine (UDMH) as precursors for Ga, P, and N, respectively. Prior to NW growth, the substrates were cleaned in acetone and isopropyl alcohol and deposited with monodisperse Au particles from colloidal solution. Annealing at 550 °C under overpressure of TBP was carried out for 15 min, in order to desorb the surface oxide and form liquid Au-Ga droplets. Subsequently, NWs were grown with a TMGa molar fraction of $\chi_{TMGa} = 6.16 \times 10^{-5}$ and a TBP/TMGa ratio of 10. The applied growth temperatures range from 500 to 550 °C, and UDMH:TBP ratios between 0:1 (i.e., pure GaP) and 9:1 were investigated. If not explicitly stated otherwise, the duration of growth was 16 min and the Au-particle size 50 nm. During the whole process, the reactor pressure was 50 mbar with a total gas flow of 3.4 l/min, which was provided by H_2 as carrier gas. All specified temperatures were measured by a thermocouple within the graphite suszeptor.

The samples were characterized by means of high-resolution scanning electron microscopy (SEM, Hitachi S 4800-II). Two of the samples were selected for microscopic and spectroscopic investigation with transmission electron microscopy (TEM). The TEM samples were mechanically dry-transferred on lacey carbon grids. TEM studies were performed on a ThermoScientific Titan^3 Themis operating at 200 kV. The microscope is equipped with ultra-bright X-FEG electron source and spherical aberration correctors in both illumination and imaging sides. Electron energy loss spectra were recorded using the attached GIF Quantum ERS in diffraction mode with a collection angle of ~ 3 mrad, which is optimized for detection of the N-K edge at 403 eV. For Raman spectroscopy, the NWs were transferred by the same means on Si substrates. A green 532-nm laser with 400 μW was used as the excitation source and focused with a × 50 objective. The signal was analyzed with a cooled Si charge-coupled device (CCD) detector.

Results and Discussion

Morphology

In Fig. 1, the morphologies of differently prepared GaP(N) NWs are shown. Note that the bending and touching of NWs with very high aspect ratio was not present right after growth, but is due to electrostatic attraction during SEM investigation [35]. The same effect additionally leads to a distortion at the top of some NWs (cf Fig. 1b, c).

The microscopic images reveal that for all parameters investigated in this study, growth of freestanding NWs has been achieved. Moreover, in most cases, all NWs are straight and vertical to the substrate as well as homogenous in length. In contrast to self-catalyzed dilute nitride NWs [14, 18, 19], no parasitical island growth was observed. These NW properties are considered essential to match the common demands for their use in applications. Besides, it can be seen that both the temperature and the UDMH concentration (expressed as UDMH:TBP ratio) have a tremendous impact on the NW morphology: increasing the temperature leads to a length reduction and enhances parasitic vapor-solid (VS) growth on the NW side facets. Both effects intensify NW tapering. Tapering is generally undesired, as the parasitic shell can degrade the functionality of devices for reasons of geometry, different compositions [36], and/or doping levels or even doping directions [37]. From the equal growth duration of all samples follows that, the axial growth rate (GR) decreases with temperature, while the coaxial GR increases. The impact of increasing UDMH concentrations, in contrast, is generally beneficial: with increasing UMDH ratio the axial GR rises, while the radial GR declines. Hence, tapering is drastically reduced—particularly for higher temperatures. Apart from that, very high UDMH ratios of 9:1 lead to unstable growth conditions. This

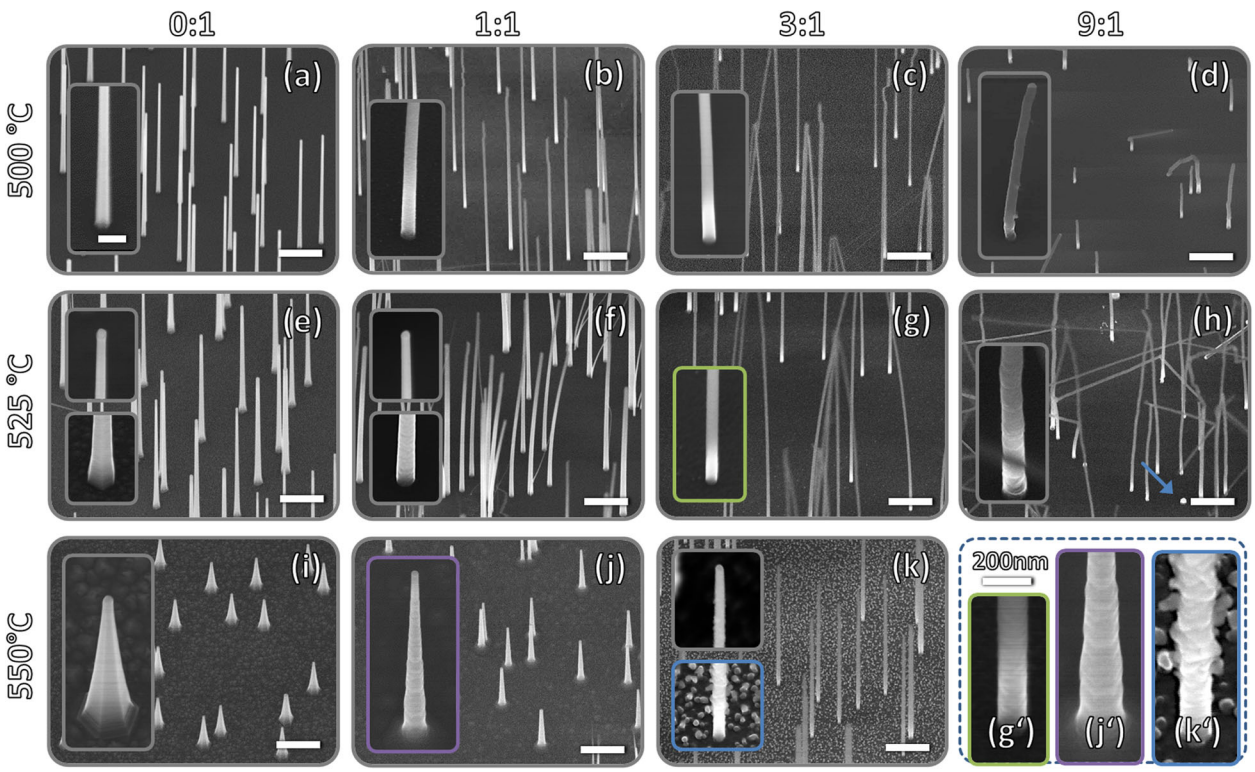

Fig. 1 VLS-grown GaP(N) nanowires on GaP(111)B. UDMH:TBP ratio and temperature were varied from 0 to 9 and 500 to 550 °C, respectively. The growth time was always 16 min. All overview and close-up scans were taken at 30° tilt and have the same scale, respectively, with the measuring bars being 2 μm or 200 nm. In (g′), (f′), and (k′) enlarged close-ups are shown for a clear visibility of the surface

instability is reflected in a frequent change of the growth direction and a wide length dispersion—partially, NW growth is even completely suppressed (see arrow in Fig. 1h). Another feature of NW growth with high UDMH ratios is surface roughening, which is exacerbated both by higher temperature and higher UDMH supply (compare images g′, j′ ,and k′). At 550 °C and a concentration of 3:1 (k and k′), where the surface is the roughest, it becomes evident that the roughening decreases from bottom to top and does not occur immediately below the Au particle. This proves that this effect is not related to the VLS growth but to the parasitic shell growth instead. The reason for this roughening might be strain due to a strong and possibly inhomogeneous incorporation of nitrogen [38] into the shell.

An evaluation of the geometric characteristics of the NWs, which is presented in Fig. 2, illustrates the tendencies described above. While the axial GR (a) increases with supply of UDMH and decreases with temperature, it is the direct opposite for the coaxial GR (b). Accordingly, the tapering parameter (c), which is defined as the difference of the radius at the top and the bottom divided by the NW length, is low for high UDMH ratios and low temperatures. Note that this definition of the tapering parameter is equal to the ratio between coaxial and axial GR.

This increase of tapering with temperature is a prevalent phenomenon in NW growth and can be explained as follows [39]: At low temperatures (≤ 500 °C), VS growth is kinetically limited, while VLS growth is only limited by the mass transport of the growth species. As the temperature increases, the kinetic barrier of VS growth is increasingly traversed, so that the coaxial GR rises. Since the VS and VLS growth compete for material, the temperature increase causes a simultaneous decrease in the axial GR. This effect can be further enhanced by an increased desorption rate and the concomitant reduction of the diffusion length. As TMGa is already fully pyrolyzed at 450 °C [40] and it is TMGa which limits the GR at V/III = 10, decomposition kinetics should play a minor role. It should be noted though that generally, besides temperature, the III–V ratio and absolute precursor flow have a tremendous impact on growth kinetics, so that tapering free NWs can be achieved also at high temperature (see, e.g., [41] for WZ-GaAs NWs and [42] for InP-NWs).

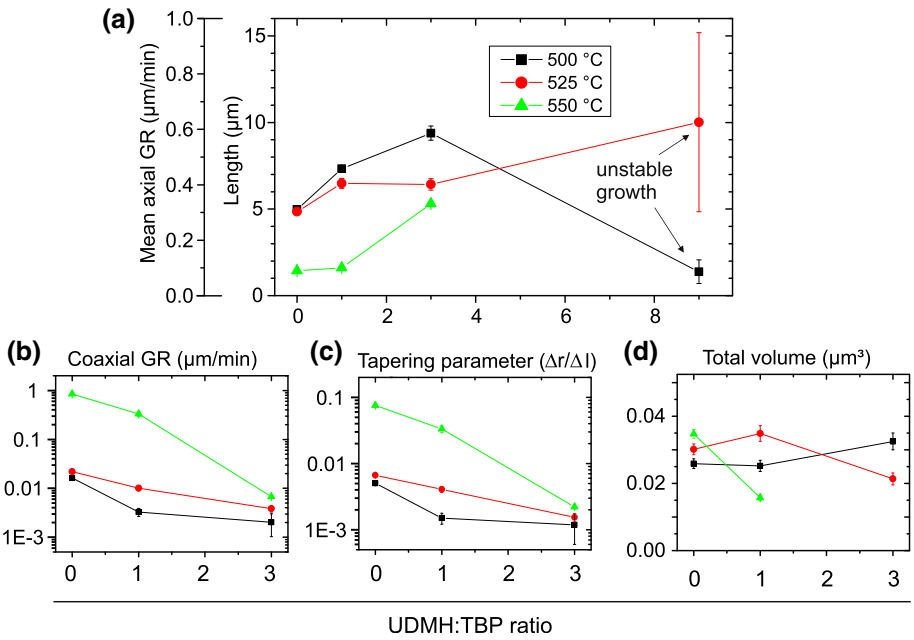

Fig. 2 Geometric characteristics of the NWs from Fig. 1 as a function of growth temperature and UMDH:TBP ratio: (**a**) length and mean axial growth rate, (**b**) coaxial growth rate, (**c**) tapering parameter, (**d**) total volume. Each measurement point represents an averaging of 10 to 20 NWs with the error bar representing the standard deviation or error propagation. The mean total volume of a NW in (**d**) was estimated assuming a truncated cone with circular cross-section

In the following, the decrease in tapering caused by the addition of UDMH is discussed. From Fig. 2a and b, it is evident that it is both due to accelerated axial VLS growth and decelerated coaxial VS growth. A similar impact on the GR is observed for the addition of HCl [33, 43] or tert-butyl-chloride (TBCl) [44] during NW growth. In both cases, the VS growth on the side facets is reduced or completely suppressed by a corrosive effect of the chlorine species [45–47]. At the same time, the axial GR increases (at least for low HCl or TBCl concentrations). It is argued that the portion of the group III species, which would contribute to VS growth in the absence of the Cl species, contributes to VLS growth instead, probably in the form of InCl for InP NWs [33]. While in these studies, the increase of Cl species always involves a decrease in the NW volume [33, 44], the volume of the GaP(N) NWs investigated here depends comparatively little on the concentration of UDMH and in some cases even increases with the UDMH concentration (Fig. 2d). For this reason, an etching effect of UDMH is very unlikely. Instead, UDMH and its fragments could sterically hinder VS growth on the side facets. There is strong evidence that a large amount of UDMH and its fragments are present as adsorbates on the NW side facets between 500 °C and 550 °C. This evidence includes the following points: first, the incomplete decomposition of UDMH, which should be proceeded by only about 5% to 30% between 500 and 550 °C [48–51]; secondly, the high concentration of UDMH in the gas phase, which equals 10 to 90 times the amount of TMGa; thirdly, experiments with in situ spectroscopy on GaPN layers, which indicate that UDMH and its fragments attach to the surface after growth and cooldown (below 650 °C), whereas this is not the case for TBP and its fragments [52]. These adsorbates prevent the Ga species from reaching the NW facets and contributing there to VS growth. Instead, they diffuse to the Au particle where they promote VLS growth. VLS growth will be significantly less affected by steric hindrance, since the surface of the Au particle acts as collector and measures about 3 times the growth front (interface between Au particle and NW). In addition, a catalytic effect of Au [53, 54] may favor the pyrolysis of UDMH and thereby promote the removal of the more volatile fragments.

Raman Spectroscopy

In order to investigate nitrogen incorporation and structural properties, Raman spectroscopy was carried out on individual NWs in the back scattering geometry. The NWs analyzed with Raman spectroscopy differ from the NWs shown in Fig. 1, in that they have a larger diameter (100 nm) and were grown only for 8 min. This ensures that the influence of parasitical VS overgrowth is negligibly small. For example, for a UDMH ratio of 3:1, the shell's percentage of the cross-sectional

area in the middle of the wire (where measurements were carried out) is less than 3%. As a reference, a lattice-matched $GaP_{1-x}N_x$ layer on Si (100) with $x = 2.1\%$ was measured, too. All spectra are normalized with respect to the longitudinal optical (LO) mode of GaP.

All spectra exhibit GaP-like transversal optical phonon modes (TO_Γ) at 365 cm^{-1} and longitudinal optical phonon modes (LO_Γ) at 399–403 cm^{-1}, which are based on Raman scattering at phonons in the center of the Brillouin zone (Γ point). In addition, spectral components near 387 cm^{-1} (X), at 397 cm^{-1} (SO), around 500 cm^{-1} (NLVM), and the LO mode of the Si substrate (LO^{Si}) at 522 cm^{-1} were observed. The 750–820 cm^{-1} range contains modes from second-order Raman scattering (SORS).

At low UDMH:TBP ratios (0.1 and 0.3), surface optical (SO) phonons at 397 cm^{-1} are observable [55–57]. This surface activated phonon mode can arise from diameter modulation [55], rough surfaces [56], and/or structural defects [57]. With increasing UDMH ratios, the SO mode either vanishes or gets superimposed by a mode referred to as X (sometimes denoted as LO_X). Its occurrence is commonly explained by a break of the translational symmetry [58–60], which in our case will be caused by insertion of N into the GaP matrix. This causes relaxation of the momentum conservation rules and thereby allows zone-boundary longitudinal optical phonon scattering due to phonons at or near the X point [59, 61]. As the X mode steadily increases with the UDMH ratio, it can be concluded that the incorporation rises, too [61–63]. Unfortunately, the intensity of the X mode does not allow for a quantification of the N content, since its exact relation with the N content is unknown and strongly depends on measurement conditions. In contrast, the intensity of the N-related local vibrational mode (NLVM) at ~ 500 cm^{-1} scales almost linearly with the concentration of (substitutional) nitrogen x, if $x \leq 2.1\%$ and spectra are normalized to the LO mode [58]. Since the NLVM is caused by vibrations of Ga–N bonds, it only reflects substitutional nitrogen [62, 64, 65]. Note that NLVM sometimes is denoted as LO_2. With the planar $GaPN_{0.021}$ reference being measured under the same conditions, the substitutional N concentration of the GaP(N) NWs can be determined from the $NLVM/LO_\Gamma$ area ratio. Due to the overlapping LO mode of Si, peak deconvolution has to be applied. It yields $NLVM/LO_\Gamma(GaPN) = 0.44 \pm 0.03$ and $NLVM/LO_\Gamma(NW,3:1) = 0.145 \pm 0.028$. Accordingly, a substitutional N-concentration of $x_{3:1} = (0.7 \pm 0.2)\%$ for an UDMH:TBP ratio of 3:1 is determined. For lower UDMH ratios, however, the intensity of the NLVM is too low for quantification.

As mentioned in the introduction, previous attempts by Suzuki et al. to incorporate N during Au-catalyzed VLS growth (of GaAs(N) NWs) failed [34]. Even if the reasons can be manifold, we consider the growth sequence to be the greatest difference (with respect to our study) and, thus, the most likely source for the failure. Suzuki et al. applied pulsed-jet epitaxy, where each of the precursors is offered separately for several seconds (referred to as pulse). Since for VLS growth the species have to travel a longer distance compared to layer growth and incorporation into the crystal is delayed through the liquid seed particle, mass transport and desorption will play a critical role. In this context, also the type of precursor and its decomposition kinetics will be crucial—as we observe in our study (cf. Figure 2).

Furthermore, increasing UDMH ratios lead to an enhancement of second-order Raman processes (SORS). This is remarkable because for planar GaPN the opposite is the case. There, N incorporation causes a strong quenching and broadening of SORS peaks [58]. This is a consequence of the high sensitivity of second-order scattering processes to lattice distortion on the scale of few lattice constants (compared to first order scattering) [58, 66]. Probable sources of such lattice distortions are N clusters and local distortion due to the short and stiff Ga–N bond [58]. Conversely, this indicates that the lattice distortion in NWs decreases with increasing UDMH concentration despite enhanced nitrogen incorporation. This could be related to a reduction of stacking faults upon UDMH supply, as both the interplanar spacing increases with hexagonality (i.e., SF density) [67] and periodicity is disturbed by each SF. Note that the normalization of the spectra on the LO_Γ is excluded as potential origin, since prior normalization the intensity of LO_Γ was about two to three times larger for N-containing structures.

TEM and EELS

In order to verify this conclusion, transmission electron microscopy (TEM) was conducted on NWs grown with and without supply of UMDH. Moreover, EELS was applied as a complementary method to prove N incorporation.

Figure 4 summarizes the TEM studies on the samples: sample 1A was grown without UDMH supply and sample 1C was grown with a UDMH:TBP ratio of 3—both samples were prepared at 500 °C. The designation follows the panel names in Fig. 1. In the EEL spectrum, the N-K edge at 400 eV is clearly seen in sample 1C, while hardly detectable in sample 1A (cf. Fig. 3a b). Both samples exhibit predominant zinc blende (ZB) structure, as can be seen from the ABCABC stacking in Fourier filtered HRTEM images of a NW luckily oriented close to the 110 zone axis (but still a couple of degrees off, cf. inset in Fig. 4c for sample 1A). Rather high densities of SFs between 150 and 200 μm^{-1} can be seen in both samples. Strikingly, in sample 1C,

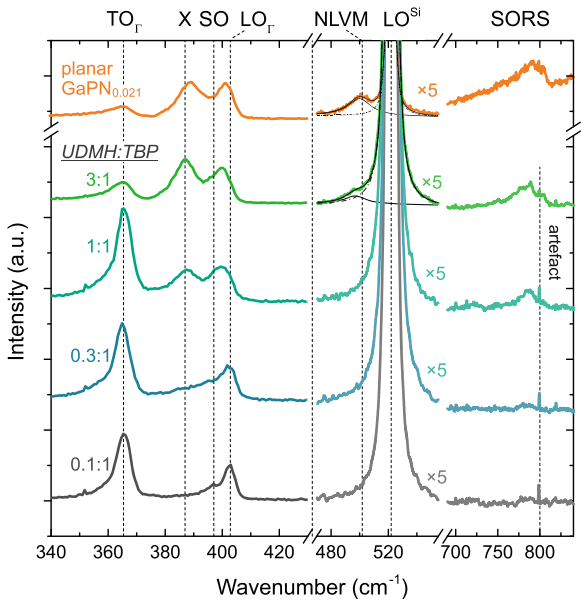

Fig. 3 μ-Raman spectra of GaP(N) NWs grown with UDMH:TBP ratios ranging from 0.1 to 3. A lattice-matched GaPN layer on Si acts as reference (orange). For the deconvolution of the NLVM component Pseudo Voigt functions (of same shape) were used. The sharp line at 800 cm^{-1} is a measurement artefact

SF-free sections of typically 150–300 nm in length can frequently be observed. Considering the similar SF densities for N-free and the N-containing NWs, it appears that it is the SF-free segments which give rise to the enhancement of the SORS processes with increasing UDMH concentrations (cf. Fig. 3).

Bright-field (BF) and dark-field (DF) imaging with various g-vectors of such SF-free segments reveal a strong strain field of single dislocations running diagonally from one end of the SF-rich region to the other (cf. Fig. 4e, f). In large angle convergent beam electron diffraction (LACBED, cf. Fig. 4g), a typical twist and splitting of the Bragg line is observed when encountering the defect line. This proves that it is indeed a dislocation, i.e., a line defect, and not a planar defect, e.g., an inclined plane boundary, because such a planar boundary would result in a shift of the Bragg line in LACBED and not in the observed twist and splitting [68]. From the inclination angle of the dislocation line, and BF-TEM images with g.b visibility criteria, the dislocations are mixed-type comprising screw and edge character. Considering that SFs are grown-in defects and that the dislocation is pinned between SFs, it is likely that the dislocation has also formed during growth and not afterwards caused by mechanical stress. This conclusion is additionally strengthened by the slightly reduced diameter within the SF-free regions. Most probably, the dislocation formation is caused by

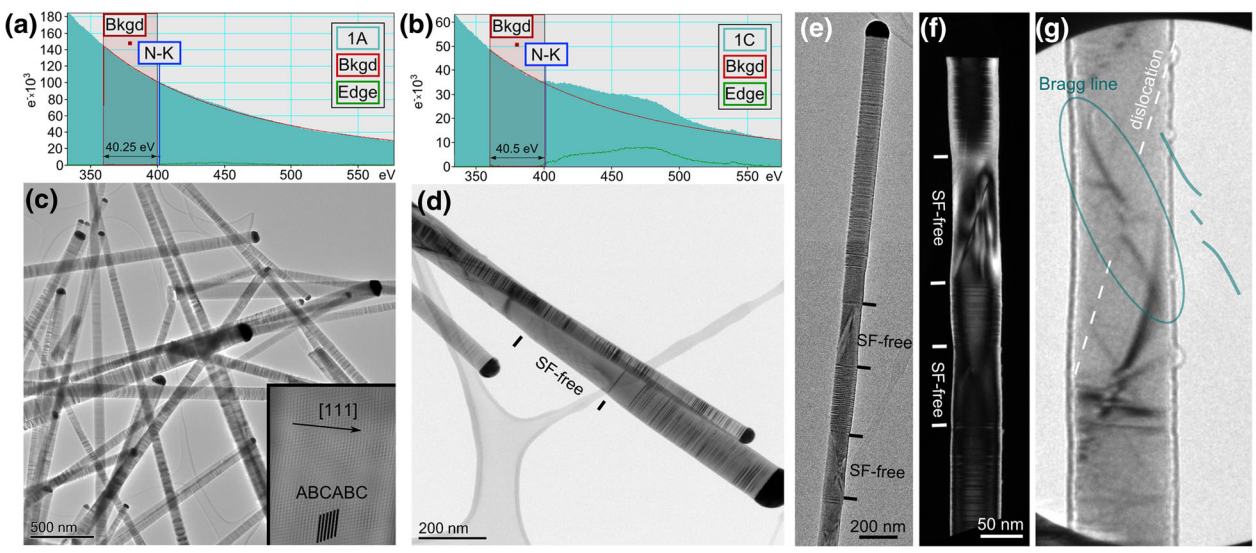

Fig. 4 TEM results of sample 1A and 1C, grown without and with supply of UDMH, respectively. The designation follows the panel names in Fig. 1. Electron energy loss (EEL) spectrum of sample 1A (**a**) and 1C (**b**), the incorporation of N in sample 1C is clearly revealed. TEM micrographs of sample 1A (**c**) and 1C (**d**). The inset in (**c**) is a Fourier filtered HRTEM image of a small SF-free region in sample 1A. Despite that the sample is a couple of degrees off the ⟨110⟩ zone axis, the ABCABC stacking of GaP is still visible, confirming the zincblende structure. SF-free sections in sample 1C are highlighted. Bright-field (**e**) and dark-field (**f**) TEM images show strong strain contrast along the line of the diagonal of SF-free region. Typical twist and splitting of Bragg line [63] in the large-angle convergent beam electron diffraction (LACBED) pattern in (**g**) confirms the presence of dislocation in the SF-free region (highlighted in dark cyan)

high local strain due to N incorporation and the very different bond lengths of Ga–N and Ga–P.

A likely explanation for the absence of stacking faults by the presence of a dislocation is given in the following. It is known that VLS growth normally proceeds via layer-by-layer growth, where 2D nuclei determine whether the next layer will follow the stacking sequence (ZB nucleus) or forms SF (WZ nucleus). For Au-catalyzed growth, under most conditions, nuclei form at the triple phase boundary [39]. In this case, nucleation barriers of ZB and WZ are very close, leading to frequent SF formation, as also observed in the investigated NWs.

With the presence of a dislocation, the growth mechanism is significantly altered, leading to preferred incorporation of material in the vicinity of the dislocation core. Here, the two characters of a dislocation have to be considered. The screw character gives rise to protruding atoms (out of the flat {111} surface) acting as preferred incorporation sites for atoms transforming from liquid to solid. The spiral arrangement of atoms along the dislocation line (cf. Refs. [69, 70]) dictates the stacking sequence, which is defined when the dislocation nucleates. Only when the dislocations runs out, stacking disorder is again possible. The reason why the dislocation exists still inside the nanowire is likely the anisotropic stress field in the radial direction of its edge component, which is compressive at one side and tensile at the other one. This gives rise to a net force dragging the dislocation during growth towards the center, and finally to the other edge of the NW in a diagonal manner. The straight course of it is a result of the dislocation line tension.

Conclusion

We have shown how to incorporate dilute amounts of nitrogen into GaP NWs during Au-catalyzed VLS growth and have demonstrated impacts on the crystalline structure of GaP(N) NWs. Raman spectroscopy proves increasing amounts of N with rising supply of the nitrogen precursor UDMH and verifies incorporation at group V sites. Studying a wide range of UDMH concentrations and temperatures, we found an overall advantageous impact of UDMH on the morphology. This is reflected in reduced NW tapering, which we attribute to steric hindrance of incompletely pyrolized UDMH molecules. TEM analysis reveals zinc blende structure in both N-free and N-containing NWs with a rather high stacking fault (SF) density. Strikingly, N-containing NWs exhibit 150–300 nm long regions without any SFs, which are interspersed with individual dislocations. It seems that these dislocations are formed during NW growth and suppress SF nucleation. This study demonstrates the suitability of the common N-precursor UDMH for N incorporation in VLS-grown NWs and will enable further tailoring of the NW material properties.

Abbreviations

BF: Bright-field; DF: Dark-field; EELS: Electron energy loss spectroscopy; GR: Growth rate; LACBED: Large angle convergent beam electron diffraction; MBE: Molecular beam epitaxy; MOVPE: Metalorganic vapor phase epitaxy; NLVM: Nitrogen-related local vibrational mode; NW: Nanowire; SEM: Scanning electron microscopy; SF: Stacking fault; SORS: Second-order Raman scattering; TBP: Tertiarybutylphosphine; TEM: Transmission electron microscopy; TMGa: Trimethylgallium; UDMH: Unsymmetrical dimethyl hydrazine; VLS: Vapor-liquid-solid; VS: Vapor-solid; WZ: Wurtzite; ZB: Zinc blende

Acknowledgements

We thank K. Schwarzburg for use of the Raman spectroscopy setup and his support during the measurements. We are grateful for A. Müller for technical support of the MOVPE system and A. Nägelein for discussion.

Funding

We acknowledge support for the Article Processing Charge by the German Research Foundation and the Open Access Publication Fund of the Technische Universität Ilmenau. MW and ES acknowledge financial support by the German Research Foundation through the Research Training Group GRK1896 "In situ microscopy with electrons, X-rays and scanning probes" and the Cluster of Excellence EXC315 "Engineering of Advanced Materials".

Availability of Data and Materials

The datasets generated during and/or analyzed during the current study are available from the corresponding author on reasonable request.

Authors' Contributions

MS conceived and designed the experiments as well as performed and interpreted the Raman spectroscopy and geometrical analysis. MW conducted the TEM and EELS study. KP prepared the samples. PK, ES, TH supervised this work and co-wrote the manuscript. All authors read and approved the final manuscript.

Competing Interests

The authors declare that they have no competing interests.

Publisher's Note

Author details

[1]Department of Photovoltaics, Institute of Physics and Institute of Micro- and Nanotechnologies, Technische Universität Ilmenau|, 98693 Ilmenau, Germany. [2]Institute of Micro- and Nanostructure Research & Center for Nanoanalysis and Electron Microscopy (CENEM), Department of Materials Science, Friedrich-Alexander-Universität Erlangen-Nürnberg, 91058 Erlangen, Germany.

Received: 14 August 2018 Accepted: 9 December 2018
Published online: 29 December 2018

References

1. Joyce HJ, Gao Q, Hoe Tan H et al (2011) III–V semiconductor nanowires for optoelectronic device applications. Prog Quantum Electron 35:23–75
2. Hyun JK, Zhang S, Lauhon LJ (2013) Nanowire heterostructures. Annu Rev Mater Res 43:451
3. Tomioka K, Fukui T (2014) Recent progress in integration of III–V nanowire transistors on Si substrate by selective-area growth. J Phys D Appl Phys 47:394001
4. Dasgupta NP, Sun J, Liu C, Brittman S, Andrews SC, Lim J, Gao H, Yan R, Yang P (2014) 25th anniversary article: semiconductor nanowires - synthesis, characterization, and applications. Adv Mater 26:2137–2183
5. Glas F (2015) Strain in nanowires and nanowire heterostructures. In: Fontcuberta i, Morral A, Dayeh SA, Jagadish C (eds) Semicond. Nanowires I Growth Theory (Semiconductors Semimetals, Vol. 93), 1st edn. Elsevier Inc, Waltham, San Diego, Oxford, London, pp 79–123

6. Tomioka K, Motohisa J, Hara S, Fukui T (2008) Control of InAs nanowire growth directions on Si. Nano Lett 8:3475–3480
7. Vurgaftman I, Meyer JR (2003) Band parameters for nitrogen-containing semiconductors. J Appl Phys 94:3675–3696
8. Ayşe E (2008) Dilute III-V nitride semiconductor and material systems. Springer-Verlag, Berlin Heidelberg New York
9. Shan W, Walukiewicz W, Yu KM, Wu J, Ager JW, Haller EE, Xin HP, Tu CW (2000) Nature of the fundamental band gap in GaNxP1-x alloys. Appl Phys Lett 76:3251–3253
10. Buyanova IA, Pozina G, Bergman JP, Chen WM, Xin HP, Tu CW (2002) Time-resolved studies of photoluminescence in GaNxP1−x alloys: evidence for indirect-direct band gap crossover. Appl Phys Lett 81:52–54
11. Deutsch TG, Koval CA, Turner JA (2006) III-V nitride epilayers for photoelectrochemical water splitting: GaPN and GaAsPN. J Phys Chem B 110:25297–25307
12. Deutsch TG, Head JL, Turner JA (2008) Photoelectrochemical characterization and durability analysis of GaInPN epilayers. J Electrochem Soc 155:B903
13. Seo HW, Bae SY, Park J, Kang M, Kim S (2003) Nitrogen-doped gallium phosphide nanowires. Chem Phys Lett 378:420–424
14. Kuang YJ, Sukrittanon S, Li H, Tu CW (2012) Growth and photoluminescence of self-catalyzed GaP/GaNP core/shell nanowires on Si (111) by gas source molecular beam epitaxy. Appl Phys Lett 100:053108
15. Ahn N, Araki Y, Kondow M, Yamaguchi M, Ishikawa F (2014) Effects of growth interruption, As and Ga fluxes, and nitrogen plasma irradiation on the molecular beam epitaxial growth of GaAs/GaAsN core–shell nanowires on Si (111). Jpn J Appl Phys 53:065001
16. Araki Y, Yamaguchi M, Ishikawa F (2013) Growth of dilute nitride GaAsN/GaAs heterostructure nanowires on Si substrates. Nanotechnology 24:065601
17. Kasanaboina PK, Ahmad E, Li J, Reynolds CL, Liu Y, Iyer S (2015) Self-catalyzed growth of dilute nitride GaAs/GaAsSbN/GaAs core-shell nanowires by molecular beam epitaxy. Appl Phys Lett. https://doi.org/10.1063/1.4930887
18. Sukrittanon S, Dobrovolsky A, Kang W-M, Jang J-S, Kim B-J, Chen WM, Buyanova IA, Tu CW, Kuang YJ (2014) Growth and characterization of dilute nitride GaNxP1−x nanowires and GaNxP1−x/GaNyP1−y core/shell nanowires on Si (111) by gas source molecular beam epitaxy. Appl Phys Lett 105:072107
19. La R, Pan JL, Bastiman F, Tu CW (2016) Self-catalyzed Ga (N) AsP nanowires and GaAsP/GaNAsP core–shell nanowires grown on Si (111) by gas-source molecular beam epitaxy. J Vac Sci Technol B, Nanotechnol Microelectron Mater Process Meas Phenom 34:02L108
20. Chen SL, Chen WM, Ishikawa F, Buyanova IA (2015) Suppression of non-radiative surface recombination by N incorporation in GaAs/GaNAs core/shell nanowires. Sci Rep 5:11653
21. Dobrovolsky A, Sukrittanon S, Kuang Y, Tu CW, Chen WM, Buyanova IA (2014) Energy upconversion in GaP/GaNP core/shell nanowires for enhanced near-infrared light harvesting. Small 10:4403–4408
22. Filippov S, Sukrittanon S, Kuang Y, Tu C, Persson POÅ, Chen WM, Buyanova IA (2014) Origin of strong photoluminescence polarization in GaNP nanowires. Nano Lett 14:5264–5269
23. Filippov S, Jansson M, Stehr JE, Palisaitis J, Persson POÅ, Ishikawa F, Chen WM, Buyanova IA (2016) Strongly polarized quantum-dot-like light emitters embedded in GaAs/GaNAs core/shell nanowires. Nanoscale 8:15939–15947
24. Buyanova IA, Chen WM, Tu CW (2004) Defects in dilute nitrides. J Phys Condens Matter 16:S3027–S3035
25. Chen WM, Buyanova IA, Tu CW, Yonezu H (2006) Point defects in dilute nitride III-N-As and III-N-P. Phys B Condens Matter 376–377:545–551
26. Geisz JF, Reedy RC, Keyes BM, Metzger WK (2003) Unintentional carbon and hydrogen incorporation in GaNP grown by metal-organic chemical vapor deposition. J Cryst Growth 259:223–231
27. Thinh NQ, Vorona IP, Buyanova IA et al (2005) Properties of Ga-interstitial defects in AlxGa1-xNyP1-y. Phys Rev B - Condens Matter Mater Phys 71:1–9
28. Janotti A, Wei S-H, Zhang SB, Kurtz S, Van de Walle CG (2003) Interactions between nitrogen, hydrogen, and gallium vacancies in GaAs1−xNx alloys. Phys Rev B - Condens Matter Mater Phys 67:161201(R)
29. Dagnelund D, Buyanova IA, Wang XJ, Chen WM, Utsumi A, Furukawa Y, Wakahara A, Yonezu H (2008) Formation of grown-in defects in molecular beam epitaxial Ga (In) NP: effects of growth conditions and postgrowth treatments. J Appl Phys. https://doi.org/10.1063/1.2895379
30. Ghoneim H, Mensch P, Schmid H et al (2012) In situ doping of catalyst-free InAs nanowires. Nanotechnology 23:505708
31. Zhang Y, Wu J, Aagesen M, Liu H (2015) III–V nanowires and nanowire optoelectronic devices. J Phys D Appl Phys 48:463001
32. Wallentin J, Wickert P, Ek M, Gustafsson A, Reine Wallenberg L, Magnusson MH, Samuelson L, Deppert K, Borgström MT (2011) Degenerate p-doping of InP nanowires for large area tunnel diodes. Appl Phys Lett 99:253105
33. Borgström MT, Wallentin J, Trägårdh J, Ramvall P, Ek M, Wallenberg LR, Samuelson L, Deppert K (2010) In situ etching for total control over axial and radial nanowire growth. Nano Res 3:264–270
34. Suzuki H, Sakai K, Haraguchi T, Yamauchi T, Hijii M, Maeda K, Ikari T (2014) Effects of nitrogen precursor on the Au-assisted vapor–liquid–solid growth of GaAs (N) nanostructures. J Cryst Growth 386:100–106
35. Liu J, Lee S, Lee K, Ahn YH, Park J-Y, Koh KH (2008) Bending and bundling of metal-free vertically aligned ZnO nanowires due to electrostatic interaction. Nanotechnology 19:185607
36. Sun W, Guo YN, Xu HY, Liao ZM, Gao Q, Tan HH, Jagadish C, Zou J (2013) Unequal P distribution in nanowires and the planar layer during GaAsP growth on GaAs {111} B by metal-organic chemical vapor deposition. J Phys Chem C 117:19234–19238
37. Dufouleur J, Colombo C, Garma T, Ketterer B, Uccelli E, Nicotra M, Fontcuberta i, Morral A (2010) P-doping mechanisms in catalyst-free gallium arsenide nanowires. Nano Lett 10:1734–1740
38. Németh I, Torunski T, Kunert B, Stolz W, Volz K (2007) Microstructural analysis of Ga (NAs)/GaP heterostructures. J Appl Phys 101:123524
39. Dubrovskii VG (2015) Theory of VLS growth of compound semiconductors. In: Semicond. Semimetals, 1st edn, pp 1–78
40. Li SH, Buchan NI, Larsen CA, Stringfellow GB (1989) OMVPE growth mechanism for GaP using tertiarybutylphosphine and trimethylgallium. J Cryst Growth 96:906–914
41. Joyce HJ, Wong-Leung J, Gao Q, Tan HH, Jagadish C (2010) Phase perfection in zinc blende and Wurtzite III–V nanowires using basic growth parameters. Nano Lett 10:908–915
42. Yuan X, Guo Y, Caroff P, He J, Tan HH, Jagadish C (2017) Dopant-free twinning superlattice formation in InSb and InP nanowires. Phys Status Solidi - Rapid Res Lett 11:1–6
43. Assali S, Zardo I, Plissard S et al (2013) Direct band gap wurtzite gallium phosphide nanowires. Nano Lett 13:1559–1563
44. Tateno K, Zhang G, Gotoh H (2014) Etching effect of tertiary-butyl chloride during InP-nanowire growth. J Cryst Growth 402:299–303
45. Kitatani T, Tsuchiya T, Shinoda K, Aoki M (2005) In situ etching of InGaAsP/InP by using HCl in an MOVPE reactor. J Cryst Growth 274:372–378
46. Franke D, Sabelfeld N, Ebert W, Harde P, Wolfram P, Grote N (2003) Surface quality of InP etched with tertiarybutylchloride in an MOVPE reactor. J Cryst Growth 248:421–425
47. Caneau C, Bhat R, Koza M, Hayes JR, Esagui R (1991) Etching of InP by HCl in an OMVPE reactor. J Cryst Growth 107:203–208
48. Bourret-Courchesne E, Ye Q, Peters DW, Arnold J, Ahmed M, Irvine SJC, Kanjolia R, Smith LM, Rushworth SA (2000) Pyrolysis of dimethylhydrazine and its co-pyrolysis with triethylgallium. J Cryst Growth 217:47–54
49. Thieu QT, Inamoto T, Kuboya S, Onabe K (2013) Pyrolysis of dimethylhydrazine for the MOVPE growth of GaN and InN monitored by in-situ quadrupole mass spectrometry. Phys Status Solidi 10:405–408
50. Lee RT, Stringfellow GB (1999) Pyrolysis of 1,1 dimethylhydrazine for OMVPE growth. J Electron Mater 28:963–969
51. Stange H (2013) Präparation und Analyse von GaPN-Schichten auf Si (001). Humboldt-Universität zu, Berlin
52. Supplie O, May MM, Stange H, Höhn C, Lewerenz H, Hannappel T (2014) Materials for light-induced water splitting: in situ controlled surface preparation of GaPN epilayers grown lattice-matched on Si (100). J Appl Phys 115:113509
53. Salehzadeh O, Watkins SP (2011) Control of GaAs nanowire morphology by group III precursor chemistry. J Cryst Growth 325:5–9
54. Campbell CT, Sharp JC, Yao YX, Karp EM, Silbaugh TL (2011) Insights into catalysis by gold nanoparticles and their support effects through surface science studies of model catalysts. Faraday Discuss 152:227
55. Gupta R, Xiong Q, Mahan GD, Eklund PC (2003) Surface optical phonons in gallium phosphide nanowires. Nano Lett 3:1745–1750
56. Sahoo S, Hu MS, Hsu CW, Wu CT, Chen KH, Chen LC, Arora AK, Dhara S (2008) Surface optical Raman modes in InN nanostructures. Appl Phys Lett. https://doi.org/10.1063/1.3040681
57. Dobrovolsky A, Sukrittanon S, Kuang YJ, Tu CW, Chen WM, Buyanova IA (2014) Raman spectroscopy of GaP/GaNP core/shell nanowires. Appl Phys Lett 105:193102

58. Buyanova IA, Chen WM, Goldys EM, Xin HP, Tu CW (2001) Structural properties of a GaNxP1-x alloy: Raman studies. Appl Phys Lett 78:3959–3961
59. Yoon S, Seong MJ, Geisz JF, Duda A, Mascarenhas A (2003) Evolution of electronic states in GaPN studied by resonant Raman scattering spectroscopy. Phys Rev B 67:235209
60. Christian TM, Fluegel B, Beaton DA, Alberi K, Mascarenhas A (2016) Bismuth-induced Raman modes in GaP_1-xBi_x. Jpn J Appl Phys 55:108002
61. Vorlíček V, Gregora I, Riede V, Neumann H (1988) Raman scattering study of GaP:N epitaxial layers. J Phys Chem Solids 49:797–805
62. Buyanova IA, Izadifard M, Ivanov IG et al (2004) Direct experimental evidence for unusual effects of hydrogen on the electronic and vibrational properties of GaNP alloys: a proof for a general property of dilute nitrides. Phys Rev B 70:245215
63. Kaneko M, Hashizume T, Odnoblyudov VA, Tu CW (2007) Electrical and deep-level characterization of GaP1−xNx grown by gas-source molecular beam epitaxy. J Appl Phys 101:103707
64. Ulrici W, Clerjaud B (2005) A carbon-nitrogen complex in gallium phosphide. Phys Rev B - Condens Matter Mater Phys 72:1–6
65. Talwar DN (2004) Structural and vibrational properties of dilute GaNxAs1-x(P1-x). Phys E-Low-Dimensional Syst Nanostructures 20:321–324
66. Teicher M, Beserman R, Klein MV, Morkoç H (1984) Crystalline structure of mixed Ga1-xAlxAs and GaP1-xAsx crystals. Phys Rev B 29:4652–4658
67. Liu Z, Merckling C, Caymax M, Rooyackers R, Collaert N, Thean A, Richard O, Bender H, Vandervorst W, Heyns M (2015) Quantitative method to determine planar defect frequency in InAs nanowires by high resolution X-ray diffraction. Cryst Growth Des 15:3868–3874
68. Cherns D, Preston AR (1986) CBED studies of crystal defects. Proc ICEM-11. Kyoto 1:721–722
69. Morin SA, Jin S (2010) Screw dislocation-driven epitaxial solution growth of ZnO nanowires seeded by dislocations in GaN substrates. Nano Lett 10:3459–3463
70. Jin S, Bierman MJ, Morin SA (2010) A new twist on nanowire formation: screw-dislocation-driven growth of nanowires and nanotubes. J Phys Chem Lett 1:1472–1480